Investigating the Relationship Between Length of Day and El-Niño Using Wavelet Coherence Method

Shrishail Raut, Sadegh Modiri, Robert Heinkelmann, Kyriakos Balidakis, Santiago Belda, Chaiyaporn Kitpracha, and Harald Schuh

Abstract

The relationship between the length of day (LOD) and El-Niño Southern Oscillation (ENSO) has been well studied since the 1980s. LOD is the negative time-derivative of UT1-UTC, which is directly proportional to Earth Rotation Angle (ERA), one of the Earth Orientation Parameters (EOP). The EOP can be determined using Very Long Baseline Interferometry (VLBI), which is a space geodetic technique. In addition, satellite techniques such as the Global Navigation Satellite System (GNSS), Satellite Laser Ranging (SLR), Doppler Orbitography and Radiopositioning Integrated by Satellite (DORIS) can provide Earth Rotation Parameters, i.e., polar motion and LOD. ENSO is a climate phenomenon occurring over the tropical eastern Pacific Ocean that mainly affects the tropics and the subtropics. Extreme ENSO events can cause extreme weather like flooding and droughts in many parts of the world. In this work, we investigated the effect of ENSO on the LOD from January 1979 to April 2022 using the wavelet coherence method. This method computes the coherence between the two non-stationary time-series in the time-frequency domain using the real-valued Morlet wavelet. We used the Multivariate ENSO index version 2 (MEI v.2) which is the most robust series as the climate index for the ENSO, and LOD time-series from IERS (EOP 14 C04 (IAU2000A)). We also used Oceanic Niño and Southern Oscillation index in this study for comparison. The results show strong coherence of 0.7 to 0.9 at major ENSO events for the periods 2–4 years between LOD and MEI.v2.

1 Introduction

This paper discusses the impact of the major El-Niño Southern Oscillation (ENSO) events on the length of day (LOD). The relationship between ENSO and LOD is well known in the scientific community since the 1980s. Gipson (2016) suggested that the major ENSO events

S. Raut (✉) · C. Kitpracha · H. Schuh
GFZ German Research Centre for Geosciences, Space Geodetic Techniques, Potsdam, Germany

Technische Universität Berlin, Chair Satellite Geodesy, Berlin, Germany
e-mail: raut@gfz-potsdam.de

S. Modiri
Federal Agency for Cartography and Geodesy (BKG), Frankfurt, Germany

R. Heinkelmann
GFZ German Research Centre for Geosciences, Space Geodetic Techniques, Potsdam, Germany

K. Balidakis
GFZ German Research Centre for Geosciences, Earth System Modelling, Potsdam, Germany

S. Belda
Applied Mathematics Dept., UAVAC, University of Alicante, Alicante, Spain

of 1997–98 and 2016 caused a change of $750 \, \mu s \, d^{-1}$ in LOD. Also, Le Bail et al. (2014) found that there is a significant correlation between Multivariate ENSO Index (MEI) and various components of LOD. In this study, we mainly focused on the relationship between LOD and ENSO index such as Multivariate ENSO Index version 2 (MEI.v2), which is the most robust index as compared to the other indices. We also investigated the relationship between LOD and other ENSO indices, such as Southern Oscillation Index (SOI) and Oceanic Niño Index (ONI) as well, for comparison.

There are various methods which can be used to understand the relationship between LOD and ENSO. For example, previous studies have used the Singular Spectrum Analysis (SSA) method (Gross et al. 1996; Dickey et al. 2011), plain decomposition (Chao 1984, 1989), or de-trended fluctuation analysis (Alvarez-Ramirez et al. 2010). For this study, we used the wavelet coherence analysis method with several geophysical time series applications (Grinsted et al. 2004; Modiri et al. 2021; Modiri 2021). The wavelet coherence analysis technique effectively recognizes regions of high co-motion in the time-frequency domain, which helps us understand the amount of coherence at various periods between LOD and ENSO during major ENSO events. Kumar and Foufoula-Georgiou (1997) describes the wavelet analysis for geophysical applications.

2 Data

2.1 Length of Day (LOD)

The LOD is a part of the Earth Orientation Parameters (EOP) and is the negative time derivative of UT1-UTC. It is the difference between the duration of the day measured by space geodetic techniques such as Very Long Baseline Interferometry (VLBI), Global Navigation Satellite System (GNSS), and the nominal day with a duration of 86 400 TAI-compatible seconds. For this study, we use the LOD time-series, obtained from the IERS EOP 14 C04 combined solution (Bizouard et al. 2019), having a daily temporal resolution (see Fig. 1) and epoch at midnight UTC. The LOD time series used in this study spans from January 1st 1979 to April 1st 2022.

2.2 El-Niño Southern Oscillation (ENSO)

El-Niño southern oscillation (ENSO) is a coupled oceanic-atmospheric extreme weather event occurring in the eastern
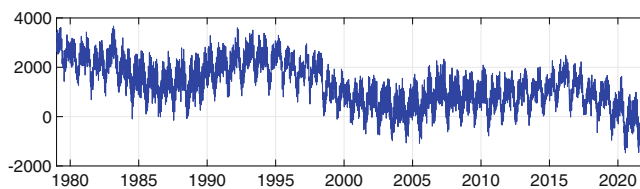
Fig. 1 LOD time-series from 1st January 1979 to 1st April 2022 (IERS EOP 14 C04), daily resolution. *(LOD values are in* $\mu s \, d^{-1}$*)*
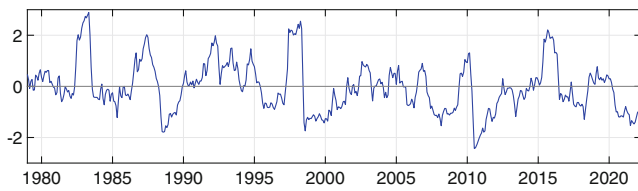
equatorial region of the Pacific ocean. It can be characterized by variations in the Sea Surface Temperature (SST) and the trade winds. The oscillations with different periods are irregular. The ENSO typically consists of three phases lasting between 2–7 years: the warming phase which is also known as El-Niño, the neutral phase, and the cooling phase, which is also known as La-Niña. The El-Nino can be divided into several categories based on where the highest tropical Pacific SST anomalies occur.

The standard El-Niño can also be categorized as the Eastern Pacific El-Niño, having the Pacific SST anomaly in the Eastern Pacific regions (near the coasts of Southern America). In the case of the other type of El-Niño, known as the Central Pacific (CP) El-Niño, the Pacific SST anomaly occurs in the Central Pacific region (near the International dateline).

There are several indices available to quantify the ENSO activity. These include Multivariate ENSO Index (MEI.v2), Southern Oscillation Index (SOI), Oceanic Niño Index (ONI), etc. The Multi-Variate ENSO Index version 2 (MEI.v2) is the most robust index and is computed using five different parameters, namely, sea level pressure (SLP), sea surface temperature (SST), surface zonal winds (U), surface meridional winds (V), and outgoing longwave radiation (OLR) over the tropical Pacific basin (30°S–30°N and 100°E–70°W). The MEI.v2 values are provided as two-month seasons, i.e., December-January, January-February, etc. The Southern Oscillation Index (SOI) is the atmospheric component of the ENSO and is computed by the sea level pressure difference between stations in Tahiti and Darwin.[1] This index is, however noisier in comparison to the MEI.v2 index. The Oceanic Niño Index (ONI) is computed by taking a three-month running mean of SST of the equatorial region (5°N–5°S, 170°W–120°W).[2] However, in this paper, we focused on the MEI.v2 index as it is a suitable index for global parameters such as LOD. The MEI.v2 time-series

---

[1] https://psl.noaa.gov/data/correlation/soi.data.

[2] https://psl.noaa.gov/data/correlation/oni.data.

Fig. 2 MEI.v2 time-series from 1st January 1979 to 1st April 2022, monthly values *(The values are dimensionless)*

plot is illustrated in Fig. 2 using datasets[3] from Physical Sciences Laboratory (PSL).[4] The period of MEI.v2 datasets is January 1st 1979 to April 1st 2022 in the study. We focus on the three major El-Niño events that last from January 1982 to December 1983, January 1997 to December 1998, and January 2015 to December 2016. These three events had MEI.v2 indices above 2.0, which characterizes them as very strong El-Niño events.

3 Methodology

We performed a wavelet coherence analysis (WCA) between LOD and MEI.v2. The temporal resolution of the LOD time series is daily in contrast to the monthly values of the MEI.v2 index. Consequently, we re-sampled the monthly ENSO index to a daily resolution by linear interpolation to synchronize the data sets. As the original sampling of the MEI.v2 index is monthly (30 days), the Nyquist period would be equal to twice the original sampling period, i.e., two months (60 days). Therefore, we did not consider the coherence of the periods less than the Nyquist period, i.e., 60 days. Besides, we also employed WCA between LOD with SOI and ONI to see how other ENSO indices perform in contrast to MEI.v2. However, we will only discuss the important points.

3.1 Wavelet Coherence (WC) Method

This method computes the magnitude-squared wavelet coherence, i.e., the coherence between two non-stationary time series in the time-frequency plane. The WCA is grounded in the continuous wavelet transform (CWT) contrary to discrete wavelet transform (DWT). The CWT can be defined as (Torrence and Webster 1999):

$$W^X(n,s) = \sqrt{\frac{\Delta t}{s}} \sum_{n=1}^{N} x(n) \psi_0^* [\hat{n} - n] \left(\frac{\Delta t}{t} \right) \quad (1)$$

[3]https://psl.noaa.gov/enso/mei/data/meiv2.data.

[4]https://psl.noaa.gov/.

where, W denotes the CWT of a time series $x(n)$, n the time index, s the wavelet scale, N the length of the time series, Δt the time step, ψ_0 the mother wavelet function, and $*$ indicates the complex conjugate. The wavelet cross-spectrum is defined as a measure of the distribution of power of two signals and can be expressed as:

$$W^{XY}(n,s) = W^X(n,s) \, W^{Y*}(n,s) \quad (2)$$

where the $W^{XY}(n,s)$ is the joint power between the two time-series $x(n)$ and $y(n)$. We computed the squared cross-wavelet coherence function R^2, which tells us the amount of how coherent the cross-wavelet transform is in the time-frequency domain. The R^2 can be expressed through the following equation:

$$R^2(n,s) = \frac{|\, S(s^{-1} W^{XY}(n,s)) \,|^2}{S(s^{-1} \,|\, W^X(n,s) \,|^2) \times S(s^{-1} \,|\, W^Y(n,s) \,|^2)} \quad (3)$$

where S is a smoothing operator, which can be described as:

$$S(W) = S_{scale}(S_{time}(W_n(s))) \quad (4)$$

where S_{scale} is the smoothing along the scale axis of a wavelet and S_{time} the smoothing time. It is interesting to note that Eq. 1 is similar to the standard correlation coefficient equation. The wavelet coherence can be considered as a localized correlation coefficient in the time-frequency domain.

There are mainly three types of wavelets, namely, Generalised Morse, Analytical Morlet, and Bump wavelet. We chose a real-valued Morlet wavelet as it is recommended for feature extraction from geophysical signals (Grinsted et al. 2004) and for retaining phase information in the wavelet spectrum (Chao et al. 2014). Phase arrows indicate the relative phase relationship between these two series. If the phase arrows are pointing right, the two series are in phase, and if the phase arrows point towards the left, it means they are in anti-phase. In the case the phase arrows face downwards, LOD series leads the MEI.v2 index. Mathematically, a real-valued Morlet wavelet is represented as:

$$\psi(x) = C \exp(-x^2) \cos(5x) \quad (5)$$

where, C is the normalization constant.

It is important to discuss the coherence values in terms of their significance level w.r.t. the confidence level and degree of freedom (Chao and Chung 2019). We determined the statistical significance of the wavelet coherence using the Monte Carlo method. This is performed only for the values outside the cone of influence. We carried out this analysis using the MATLAB® (MathWorks®) toolbox for
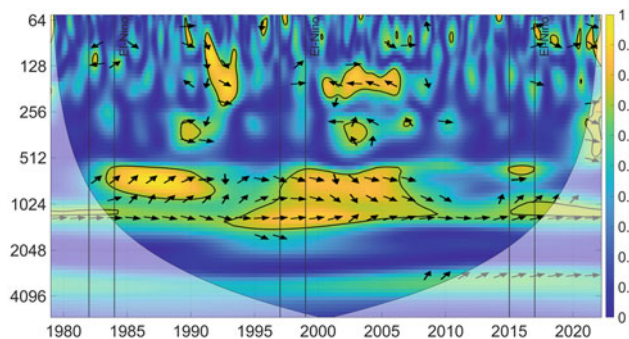
Fig. 3 Wavelet Coherence between LOD and MEI.v2. Plot description: The left y-axis is the period (in days) and the color bar corresponds to Magnitude-Squared Coherence. The vertical solid lines represent the three major ENSO events of El-Niño. The line that separates the white-faded portion and the remaining plot represents the Cone of Influence. The enclosed region by contour lines indicate the statistically significant regions (5% significance level against red noise). The arrows represent the phase information

Table 1 Coherence between LOD and MEI.v2 for ENSO event of 1982–83

Period (in days)	Coherence
111	0.76
117	0.77
124	0.75
628	0.75
666	0.77
706	0.77

performing cross wavelet and wavelet coherence analysis[5] provided by Grinsted et al. (2004).

4 Result and Discussion

This section discusses the coherence of MEI.v2 index and LOD for the periods ranging from around 600 (1.6 years) to 1500 days (4 years) as these periods show high coherence. The coherence between LOD and MEI.v2 index is illustrated in Fig. 3. We will only discuss the regions that are statistically significant (surrounded by black contour lines). The coherence between LOD with SOI and ONI is also discussed briefly.

4.1 El-Niño Event of 1982–83

In this case, the ENSO event lasted for approximately nine months (MEI.v2 > 2). From the Fig. 3, we can observe a strong coherence between LOD and ENSO starting from the middle of the event interval. Table 1 indicates a strong coherence of more than 0.75, for the periods from approximately 593 to 792 days. An interesting fact to note is that we also observe a continual strong coherence up to the year 1992 for the periods from 593 to 792 days. The occurrence of medium to strong ENSO events in 1987–88 and 1991–92 could be a reason. In addition, looking at the phase information, the ENSO seems to lead the LOD by 45°. We also observe a strong coherence of 0.76 at the shorter periods of 111 to 124 days shortly before the ENSO reaches its peak. The phase

information indicates that LOD and ENSO have an anti-phase during these periods.

For LOD and ONI, we observed periods and phase information similar to LOD and MEI.v2. However, in the case of LOD and SOI, we observed high coherence for the periods of around one year, and the phase information is opposite as compared to LOD and MEI.v2.

4.2 El-Niño Event of 1997–98

This El-Niño event is widely considered as one of the most powerful El-Niño recorded in history. The MEI.v2 index remains above 2 for 12 months. We can see from the Fig. 3 that there is a strong coherence between LOD and MEI.v2 mainly at longer periods. As from Table 2, we observe coherence between 0.75 and 0.85 for the periods from 706 to 1120 days. A much higher coherence of more than 0.85 is seen for periods 1187 to 1332 days. Besides, LOD and ENSO are almost in phase for periods from 706 to 1332 days. For the period of 62 days, the coherence is approximately 0.80. This coherence occurred shortly before the ENSO reached its maximum. We do not find any reliable phase information for these periods. An interesting fact to be noted is that the coherence between ENSO and LOD continues until the year 2009, even though there were no more strong El-Niños during these years.

In the case of LOD and ONI, we observed strong coherency and the phase information at similar periods as in LOD and MEI.v2. For LOD and SOI, we noticed strong coherency at periods of approximately two to four years. However, both the parameters are anti-phase.

Table 2 Coherence between LOD and MEI.v2 for ENSO event of 1997–98

Period (in days)	Coherence	Period (in days)	Coherence
62	0.79	998	0.75
666	0.74	1057	0.77
706	0.77	1120	0.81
748	0.78	1187	0.86
792	0.78	1280	0.87
839	0.77	1332	0.85

[5] https://noc.ac.uk/business/marine-data-products/cross-wavelet-wavelet-coherence-toolbox-matlab.

Table 3 Coherence between LOD and MEI.v2 for ENSO event of 2015–16

Period (in days)	Coherence
593	0.77
628	0.76

4.3 El-Niño Event of 2015–16

In this case, the MEI.v2 index is above 2 only for two months (September to October 2015). We observe a strong coherence between LOD and MEI.v2 of approximately 0.77 for the periods of 593 to 628 days (Table 3). The phase information is insufficient for drawing conclusions. We do not observe any coherence between LOD and ENSO after the ENSO event dissipated unlike to the previous two ENSO events. The reason could be the relatively smaller intensity and duration of ENSO.

We can see strong coherency between LOD and ONI at around two years, and the phase information is insufficient to derive any conclusions. In the case of LOD and SOI, we cannot observe any strong coherency, and subsequently, no phase information is available.

5 Conclusions

Although the relationship between LOD and ENSO has been studied extensively in the past, using the wavelet coherence method reveals a complex interaction between these two data sets (Fig. 3; Tables 1, 2, 3). The ENSO events of 1982–83 and 1997–98 show a strong coherence with LOD. In contrast, the ENSO event of 2015–16 does not show strong coherence with LOD despite having only slightly less strength as the previous two ENSO events. This indicates that the strength of an ENSO event is not the only factor affecting LOD, and the duration of the ENSO might be an important factor as well.

In the 1982–83 ENSO event, we saw a strong coherence of more than 0.75 for periods 593 to 792 days and coherence of 0.76 for periods 111 to 124 days between LOD and MEI.v2. Concerning the phase information, we observed ENSO leading LOD by 45° for a longer period and anti-phase between them for shorter periods. Another important observation is that the strong coherence between LOD and ENSO continued until 1992. The main reason could be the longer duration of the ENSO event and the ENSO events of 1987–88 and 1991–92.

During the 1997–98 ENSO event, we saw a strong coherence between LOD and MEI.v2 from 0.75 to 0.85 for periods 706 to 1120 days. For periods 1187 to 1332 days, we observed stronger coherence above 0.85. The LOD and ENSO were in phase for these long periods. The coherence

for period of 62 days was around 0.80. However, we did not find definitive phase information for these shorter periods.

For the recent 2015–16 ENSO event, we observed the coherence between LOD and MEI.v2 of 0.77 and 0.80 for periods 593 to 628 days and 41 to 52 days, respectively. We cannot conclude regarding the phase due to insufficient information.

We also performed WCA between LOD with ONI and SOI for comparison. ONI can be used as an alternative ENSO index to MEI.v2 for performing WCA with LOD. We do not recommend using SOI for WCA with LOD, as it did not show any coherency during the 2015–16 ENSO event. SOI could be only sensitive to extreme ENSO conditions that last for a longer duration.

Figure 3 shows good inter-annual coherence not only during the three significant El-Niño occurrences but also throughout the entire period, including the La-Niñas and the El-Niño off-shoots. As a result, it is evident that ENSO has a positive and negative impact on LOD, which is consistent with physics. When we look at these three ENSO events, we observe a strong coherence between LOD and ENSO at periods less than a year shortly before the ENSO reached its maximum intensity. This occurrence is common for all three ENSO events. When comparing the three ENSO events, we observe that they affected LOD at different periods despite having similar strengths. This additionally suggests that every ENSO event interacts differently with LOD. The complex behavior of coherence phasing during the different El-Niños is presumably because the three El-Niños are of different types: East-Pacific and Central-Pacific. Thus, it might be possible to understand different types of ENSO in greater depth by using its complex interaction with LOD in the future. This study could be beneficial to getting more reliable LOD models/predictions needed to meet the existing accuracy goals of global geodesy (Plag et al. 2009).

Conflict of Interest

The authors declare that they have no conflict of interest.

References

Alvarez-Ramirez J, Dagdug L, Rojas G (2010) Cycles in the scaling properties of length-of-day variations. J Geodynam 49(2):105–110. https://doi.org/10.1016/j.jog.2009.10.008

Bizouard C, Lambert S, Gattano C, Becker O, Richard JY (2019) The IERS EOP 14C04 solution for Earth orientation parameters consistent with ITRF 2014. J Geodesy 93(5):621–633. https://doi.org/10.1007/s00190-018-1186-3

Chao B (1984) Interannual length-of-day variation with relation to the southern oscillation/El Nino. Geophys Res Lett 11(5):541–544. https://doi.org/10.1029/GL011i005p00541

Chao BF (1989) Length-of-day variations caused by El Nino-Southern Oscillation and quasi-biennial oscillation. Science 243(4893):923–925. https://doi.org/10.1126/science.243.4893.923

Chao B, Chung C (2019) On estimating the cross correlation and least squares fit of one data set to another with time shift. Earth Space Sci 6(8):1409–1415

Chao BF, Chung W, Shih Z, Hsieh Y (2014) Earth's rotation variations: a wavelet analysis. Terra Nova 26(4):260–264

Dickey JO, Marcus SL, de Viron O (2011) Air temperature and anthropogenic forcing: Insights from the solid Earth. J Climate 24(2):569–574. https://doi.org/10.1175/2010JCLI3500.1

Gipson J (2016) El Nino and VLBI Measured Length of Day. In: Behrend D, Baver KD, Armstrong KL (eds) IVS 2016 general meeting proceedings: New Horizons with VGOS, p 336

Grinsted A, Moore JC, Jevrejeva S (2004) Application of the cross wavelet transform and wavelet coherence to geophysical time series. Nonlinear Process Geophys 11(5/6):561–566. https://doi.org/10.5194/npg-11-561-2004

Gross RS, Marcus SL, Eubanks TM, Dickey JO, Keppenne CL (1996) Detection of an ENSO signal in seasonal length-of-day variations. Geophys Res Lett 23(23):3373–3376. https://doi.org/10.1029/96GL03260

Kumar P, Foufoula-Georgiou E (1997) Wavelet analysis for geophysical applications. Rev Geophys 35(4):385–412. https://doi.org/10.1029/97RG00427

Le Bail K, Gipson JM, MacMillan DS (2014) Quantifying the correlation between the MEI and LOD variations by decomposing LOD with singular spectrum analysis. In: Earth on the edge: Science for a sustainable planet. Springer, pp 473–477. https://doi.org/10.1007/978-3-642-37222-3_63

Modiri S (2021) On the improvement of earth orientation parameters estimation : using modern space geodetic techniques. Doctoral thesis, Technische Universität Berlin, Berlin. https://doi.org/10.14279/depositonce-11975

Modiri S, Heinkelmann R, Belda S, Malkin Z, Hoseini M, Korte M, Ferrándiz JM, Schuh H (2021) Towards understanding the interconnection between celestial pole motion and Earth's magnetic field using space geodetic techniques. Sensors 21(22):7555

Plag HP, Rothacher M, Pearlman M, Neilan R, Ma C (2009) The global geodetic observing system. In: Advances in geosciences: Volume 13: Solid Earth (SE). World Scientific, pp 105–127

Torrence C, Webster PJ (1999) Interdecadal changes in the ENSO–monsoon system. J Climate 12(8):2679–2690